# VALIDATION OF AN UNSTEADY VORTEX LATTICE METHOD FOR HYDROFOIL CRAFT

by
Frans van Walree
Maritime Research Institute Netherlands (MARIN)
P.O. Box 28
2700 AA Wageningen
the Netherlands



## 1. Introduction

The use of high speed craft for transport of passengers and time sensitive goods has considerably increased during the last decade. Transport of passengers needs ferries with a high degree of comfort, also under less favourable weather conditions. Not only from the viewpoint of passengers, which can do without seasickness, but also from an economic viewpoint of the ferry operator. Competiveness with other means of transport, by air and by road, requires that the operational time schedule must be maintained as long as possible. Consequently, the instant that a speed reduction is necessary due to too violent motions must be postponed to ever higher sea states.

Furthermore, the use of high speed craft on confined waterways and/or with a high traffic density sets requirements to the manoeuvrability of these craft types. Manoeuvrability concerns amongst others the ability to change course and to perform an emergency stop within a specified distance. Especially for hydrofoil craft, relying on the use of a ride control system for seakeeping and manoeuvring, stringent requirements are set to the safety of operation during normal and emergency conditions. Emergency conditions include for instance ride control system failures while performing a turning manoeuvre whereby the craft assumes a certain roll angle to counteract the centrifugal forces. If one or more flaps become disabled, the craft must not capsize but must be able to resume a safe attitude.

The comfort and safety of operation should be investigated by the use of validated computer simulations since, for hydrofoil craft, performing model tests is complicated, if not impossible, and thus costly. This is due to the high speed which needs large model basins with high speed carriages and oblique wave generators, the use of ride control systems which needs expensive and complicated actuation mechanisms for flap control and the need for model scale propulsion units for self propelled tests.

For such computational methods time domain simulation methods in six degrees of freedom are required to include non-linearities and transient effects. From a hydrodynamic point of view, free surface and foil interaction effects need to be included to obtain an accurate description of forces acting on foil systems. The computational method has to be suited for handling transient and oscillatory motions simultaneously: manoeuvres are usually performed while waves are present. Furthermore, the method must be suited to take into account finite aspect ratio hydrofoil configurations with a varying planform due to taper, sweep, and dihedral angles, and the presence of supporting struts and partial span trailing edge flaps. A ride control system, actuating trailing edge flaps, needs to be included. Finally, the forward velocity of the craft is in general not constant and the influence of irregular waves needs to be considered.

In the next sections the computational method for the foil system forces is briefly described. For a more detailed description one is referred to Van Walree (1999). The last section deals with the validation of the simulation method and its components.

## 2. Unsteady hydrofoil method

### Mathematical formulation

The problem is described in the space-fixed Cartesian coordinate system, see Figure 1. A thin, finite aspect ratio lifting surface of arbitrary planform is considered that performs arbitrary motions in six degrees of freedom, below the free surface. Parts of the lifting surface may be surface piercing. Only the submerged parts are considered here, although the submergence may vary in time.

A vortex sheet exists, consisting of a bound vortex sheet representing the lifting surface and a free vortex sheet that represents the wake. The position and velocity of the bound vortex sheet are assumed to be known from the equations of motions of the hydrofoil craft.

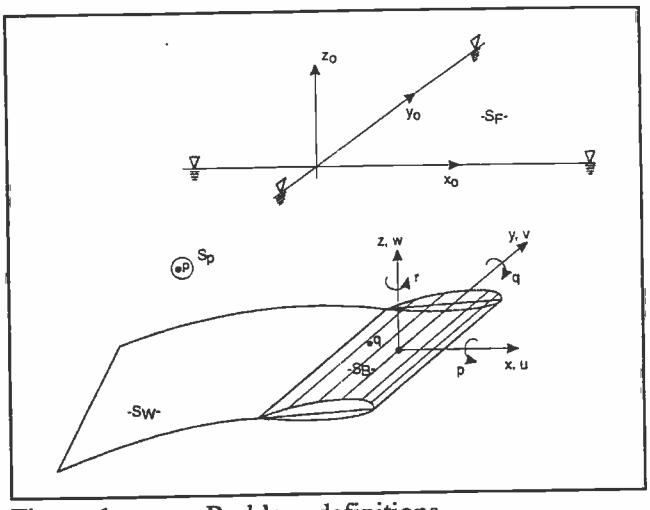

Figure 1 Problem definitions

The formulation of the problem is based on a mathematical formulation for large-amplitude ship motions by Lin and Yue (1990). Their formulation is based on the use of impulsive strength sources to represent the unsteady flow about ship hulls, here a formulation based on impulsive strength vortex elements is derived.

The motions in the fluid are described by a velocity potential $\Phi_T$:

$$\Phi_T(\underline{x}_0,t) = \Phi(\underline{x}_0,t) + \Phi_I(\underline{x}_0,t) \tag{1}$$

where $\underline{x}_0$ is the earth-fixed position vector, $t$ is time, $\Phi$ is the disturbance potential associated with the vortex sheets and $\Phi_I$ is the incident wave potential. The incident wave potential is known a priori and can be shown to satisfy the conditions in eq.'s (3) and (4). The definition of a potential function for sinusoidal waves is as follows:

$$\Phi_I = \frac{\zeta_a g}{\omega} e^{k_w z_0} \sin(k_w x_0 - \omega t) \tag{2}$$

where $\zeta_a$ is the wave amplitude, $\omega$ is the wave frequency and $k_w$ is the wave number ($k_w=\omega^2/g$).

The disturbance potential $\Phi$ satisfies the Laplace equation:

$$\nabla^2 \Phi = 0 \tag{3}$$

On the undisturbed free surface $S_F(t)$, the following linearized condition is imposed (for $t>0$):

$$\frac{\partial^2 \Phi}{\partial t^2} + g \frac{\partial \Phi}{\partial z_0} = 0 \tag{4}$$

where $g$ is the gravitational constant.

On the instantaneous lifting surface $S_B(t)$ the tangential flow condition is imposed (for $t>0$):

$$V_n = \frac{\partial \Phi}{\partial n} + \frac{\partial \Phi_I}{\partial n} \tag{5}$$

where $V_n$ is the instantaneous velocity of the lifting surface in a direction normal to its camber surface. The tangential flow condition is applied at the base plane of the lifting surface. The $\partial/\partial n$ operator denotes the derivative in normal direction, $\partial/\partial n=\underline{n}.\nabla$. The unit normal vector $\underline{n}$ is positive into the fluid domain.

The conditions at infinity ($S_\infty$) are (for $t>0$):

$$\Phi \rightarrow 0$$
$$\frac{\partial \Phi}{\partial t} \rightarrow 0 \tag{6}$$

Apart from incoming waves, the fluid is at rest at the start of the process, the initial conditions on the free surface $S_F(t)$ are then (for $t=0$):

$$\Phi = \frac{\partial \Phi}{\partial t} = 0 \tag{7}$$

The transient free surface Green's function is introduced for a submerged vortex with an impulsive strength:

$$G(p,t;q,\tau) = G^0 + G^f = \frac{1}{R} + \frac{1}{R_0} - 2\int_0^\infty [1 - \cos(\sqrt{gk}\,(t-\tau))]\; e^{k_w(z_0+\zeta)}\, J_0(k_w r)\; dk_w \tag{8}$$

for $p \neq q,\ t \geq \tau$

where $p(x_0,y_0,z_0)$ and $q(\xi,\eta,\zeta)$ are the field and singularity point coordinates respectively, $\tau$ is a past time variable, $G^0$ is the vortex plus biplane image part and $G^f$ is the free surface memory part of the Green's function, $J_0$ is the Bessel function of order zero, and

$$R = \sqrt{(x_0-\xi)^2 + (y_0-\eta)^2 + (z_0-\zeta)^2}$$
$$R_0 = \sqrt{(x_0-\xi)^2 + (y_0-\eta)^2 + (z_0+\zeta)^2} \tag{9}$$
$$r = \sqrt{(x_0-\xi)^2 + (y_0-\eta)^2}$$

A boundary integral formulation for the problem is derived by applying Green's second identity to the potential and Green's function in the fluid domain. By using the tangential flow condition, eq. (5) on the lifting surface, the following formulation may be derived, see Van Walree (1999):

$$V_{n_p} - \frac{\partial \Phi_I}{\partial n_p} = \frac{1}{4\pi}\left\{\int\int_{S_{sw}(t)} \mu(q,t)\, \frac{\partial^2 G^0}{\partial n_p \partial n_q} + \int_0^t d\tau \int\int_{S_{sw}(\tau)} \mu(q,\tau)\, \frac{\partial^3 G^f}{\partial t \partial n_p \partial n_q}\, dS\right\} \tag{10}$$

Equation (10) must be solved for the unknown doublet strength $\mu(q,t)$. A wake model needs to be established in which the vortex strength in and the location and shape of the wake sheet are specified.

**Wake model**

The Kutta condition for steady flow is that the velocity along the trailing edge of lifting surfaces remains finite. The thin wing theory equivalent is that the vortex strength at the trailing edge be zero. This is satisfied in a vortex lattice method by representing the continuous vortex distribution by a set of vortex elements with a bound vortex segment at the quarter chord position and requiring tangential flow at the three-quarter chord position of the element.

In unsteady flow the same approach can be used. At the same time vorticity must be shed from the lifting surface into the wake sheet in order to satisfy the Kelvin condition: in a potential flow the circulation $\Gamma$ around a contour enclosing the lifting surface and its wake must be conserved. By using vortex ring elements on the lifting surface and on the wake sheet as a discretization of a continuous vortex sheet and by transferring each time step the circulation at the trailing edge elements into the wake elements, this requirement is satisfied: the sum of the circulations strengths along each individual vortex line segment is always zero. Once shed, the circulation strength of wake sheet elements remains constant.

The second requirement for the wake model is that the wake sheet should be force free as it is not a solid surface; no pressure difference must be present between the upper and lower sides of the sheet. This can be accomplished by displacing the vortex element corner points with the local fluid velocity.

**Discretization**

Instead of using doublet elements for discretization of the vortex sheets, vortex ring elements carrying a circulation strength $\Gamma$ are used. These vortex elements consist of four discrete, straight vortex lines of constant strength which enclose the quadrilateral element area, see Figure 2. The induced velocity due to a vortex ring element is identical to that of a constant strength doublet element if $\Gamma=\mu$. The use of vortex ring elements satisfies the Kelvin condition while the induced velocities can be computed with a relatively small effort.

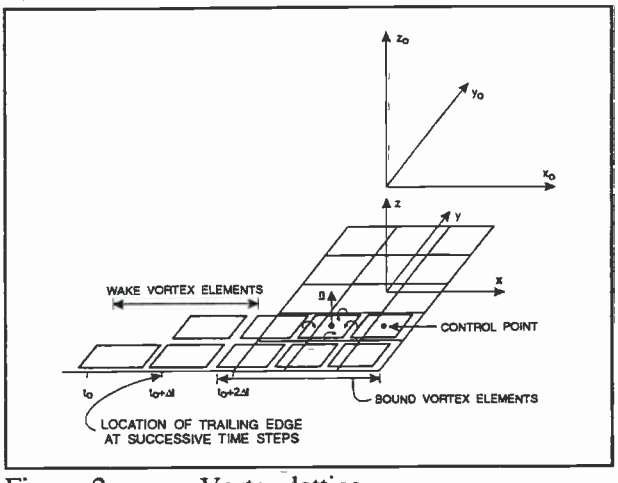

Figure 2 Vortex lattice

The vortex elements are uniformly distributed over both the chord and the span. The vortex elements are located on the base plane of the lifting surface. The leading segment of the vortex ring is placed on the element's quarter chord line. The control point where the tangential flow condition is applied is at the three-quarter point of the vortex element, at the spanwise centre. The vortex elements located at the trailing edge of the lifting surface extend to a position $\frac{1}{4}c/N$ behind the trailing edge.

**Time stepping process**

At $t$=0 the lifting surface is impulsively set into motion. At this instant, the circulation on the lifting surface is determined for the condition without wake vortex elements. The last spanwise vortex line just behind the trailing edge represents the start vortex. At each subsequent time step, the lifting surface is advanced to a new position with an instantaneous velocity. Both the position and velocity are known from the equations of motion. The gap between the instantaneous trailing edge vortex element on the lifting surface and the wake vortex element shed in the previous time step is filled with a new wake vortex element. In this way, the wake vortex element at the trailing edge has the same orientation as the flow leaving the trailing edge, to a first order approximation.

The circulation strength of the new wake vortex elements is set equal to that of the trailing vortex element of the previous time step. With a known wake vortex position and circulation, lifting surface position and velocity, the tangential flow condition, eq. (5) can be solved for the unknown circulation on the lifting surface.

**Solution of integral equation**

The discretized form of eq. (10) is given by

$$\sum_{j=1}^{NM(t)} \Gamma_j^{(t)} \iint_{S_j} \frac{\partial^2 G^0}{\partial n_{p_i} \partial n_{q_j}}(p_i,q_j)\,dS = 4\pi \underline{V}(p_i,t)\cdot \underline{n}_{p_i} -$$

$$\sum_{j=NM(t)}^{NT(t)} \Gamma_j^{(t)} \iint_{S_j} \frac{\partial^2 G^0}{\partial n_{p_i} \partial n_{q_j}}(p_i,q_j)\,dS - \Delta t \sum_{\tau=0}^{t-1} \varepsilon_\tau \{ \sum_{j=1}^{NT(\tau)} \Gamma_j^{(\tau)} \iint_{S_j} \frac{\partial^3 G^f(p_i,t;q_j,\tau)}{\partial t \partial n_{p_i} \partial n_{q_j}}\,dS \} \qquad (11)$$

where $NM$ is the number of vortex elements on the lifting surface, $NT$ is the total number of vortex elements, $t$ is the present time, $\tau$ is the past time, $i$ and $j$ are the element indices for control point $p$ and vortex element point $q$ respectively and $\varepsilon$ is an integration constant. The term on the left hand side denotes the normal induced velocity due to the vortex elements on the lifting surface, the first term on the right hand side denotes the normal velocity components due to the hydrofoil motions and the incident waves, the second term on the right hand side accounts for the normal induced velocity components due to the vortex elements in the wake while the last term contains the memory effect.

Equation (11) can be cast in a linear set of equations in the unknown circulation $\Gamma_j^{(t)}$:

$$\sum_{j=1}^{NM(t)} A_{ij} \Gamma_j^{(t)} = B_i \qquad i \equiv 1,2,\ldots,NM(t) \qquad (12)$$

where $A_{ij}$ contains the integral term of the left hand side of eq. (11) and $B_i$ contains the entire right hand side of this equation. This set of equations is solved by using common linear algebra techniques.

The evaluation of a $G^f$ term by numerical integration takes a large amount of computer time. These terms must be evaluated at each control point for the entire time history of all vortex elements. Furthermore, due to the wake shedding process, the number of vortex elements increases in time. An efficient evaluation of the $G^f$ terms is therefore of importance. For low $(t\text{-}\tau)$ values use is made of interpolation on predetermined values for $G^f$ and its derivatives. For large $(t\text{-}\tau)$ values use is made of polynomial expansions provided by Newman (1985,1992).

As a first step towards reduction of computer time and memory, the number of wake vortex elements is set to a maximum. Once this maximum number is reached, a new wake element row is still generated, but the last wake element row is removed. The maximum number of wake vortex elements must be set such that the wake sheet has a sufficient length so that the effect of removing the last wake row on the hydrofoil forces is negligible.

Next, the wake sheet position and form may be prescribed a priori: once shed, wake sheet vortex elements remains stationary. This violates the requirement of a force free wake sheet, but experience has shown that this has little effect on the forces acting on the lifting surface for practical conditions. The advantage is that induced velocities at wake element corner points need not to be computed.

The largest reduction in computer time can be obtained if the motion of the craft is assumed to be small for seakeeping problems with a constant speed and heading. The displacements of the craft around its mean position are then not taken into account in eq. (11). This will be termed the *linear* approach in the following.

Prescribing the wake sheet shape results then in a flat wake sheet in the $x_0y_0$-plane behind the lifting surface. Due to the constant speed, the relative position between a row of wake elements and the lifting surface elements is constant. The concept of influence coefficients can then be used, when determining the induced velocities due to wake sheet elements at the lifting surface control points. Only for the first

row of wake sheet elements, representing the start vortex, the influence coefficients need to be calculated each time step. Finally, a constant underwater geometry implies that the number of vortex elements on the hydrofoil configuration is constant. The influence coefficient matrix $A$ in the linear system of eq. (12) is then constant and needs to be inverted only once.

### Force evaluation

The approach taken here is based on the Kutta-Joukowsky law which implicitly accounts for the leading edge suction force by defining both the magnitude and direction of the force vector.

The Kutta-Joukowsky force components are given by:

$$\underline{F}_{kj} = \rho \underline{V} \times \underline{\Gamma} \Delta b \tag{13}$$

where $\Delta b$ is the vortex element width, and $\underline{\Gamma}$ is the circulation vector and $\underline{V}$ is the total velocity vector at the bound vortex position of the element, due to the kinematic velocity of the lifting surface and the disturbance and wave orbital motion components.

The force components associated with the time derivative of the circulation follow from:

$$\underline{F}_{t} = \rho \frac{\partial \Gamma}{\partial t} \Delta b \Delta c \cdot \underline{n} \tag{14}$$

where $\Delta c$ is the mean length of the vortex element in chordwise direction.

## 3. Validation of Hydsim

The computer program Hydsim contains a non-linear time domain simulation method in six degrees of freedom. The unsteady vortex lattice method Unvlm is used in Hydsim to determine the forces acting on the foil system. Prior to showing and validating time domain simulation results for hydrofoil craft it is useful to validate calculation results for various components relevant for the dynamic behaviour of hydrofoil craft. To this purpose comparisons will be made with model test data.

### Forces on an oscillating tandem foil system

An extensive series of measurements has been conducted at MARIN for a fully submerged, tandem foil system. The foils were each connected to six-component measurement frames which were in turn connected to a stiff beam mounted under a hydraulic oscillator fixed to the towing carriage. This set up enabled the measurement of the lift, drag and side force on each foil advancing at a constant horizontal speed while performing harmonic oscillations about a certain mean position. The phase of each separate oscillator leg could be selected arbitrarily so that heave and pitch motions could be performed. By mounting an oscillator with legs moving in the horizontal plane, a roll motion could be imposed. The centre of rotation for pitch and roll oscillations was the centre of gravity of the craft. The force components on each measuring frame can be combined into moment components about the centre of gravity of the craft.

The foil system consists of a forward and an aft foil, both of the inverted $\pi$-type. The aft foil is designed to carry about 66% of the craft weight. Figure 3 shows the foil system involved.

The calculated results are based on results obtained with the linear computational method. The foil submergence, motion amplitude and reduced frequency range are such that the differences between the linear and non-linear methods is much smaller than the scatter in the experimental data.

All force coefficients shown are normalized by the ratio between the amplitude of the oscillation velocity and the forward speed. Unsteady (interaction) effects not explained by a quasi-steady approach are then present if the force coefficient varies with the reduced frequency. The reduced frequency $k$ and velocity amplitude ratio $r$ are defined as follows:

$$k = \frac{\omega c_m}{2U}$$

$$r = \frac{\omega z_a}{U} \quad \text{heave oscillation} \qquad (15)$$

$$r = \frac{\omega \theta_a \iota}{U} \quad \text{pitch oscillation}$$

$$r = \frac{\omega \phi_a \iota}{U} \quad \text{roll oscillation}$$

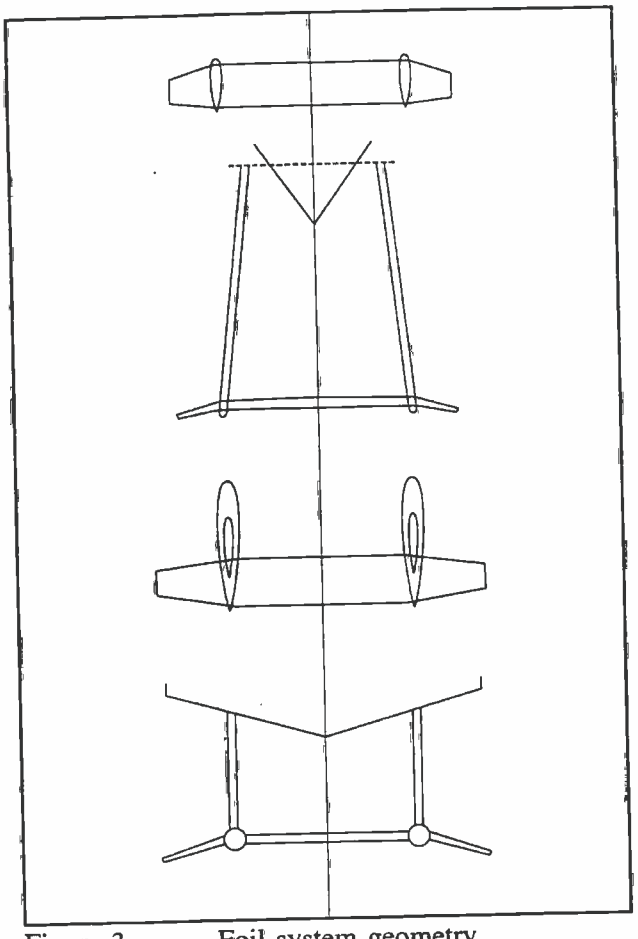

Figure 3 Foil system geometry

where $U$ is the speed of advance, $\omega$ is the frequency of oscillation, $c_m$ is the mean chord of the foils, $z_a$, $\theta_a$ and $\phi_a$ denote the heave, pitch and roll motion amplitudes respectively and $\iota$ denotes the foil spacing or main foil span for pitch and roll motions, respectively.

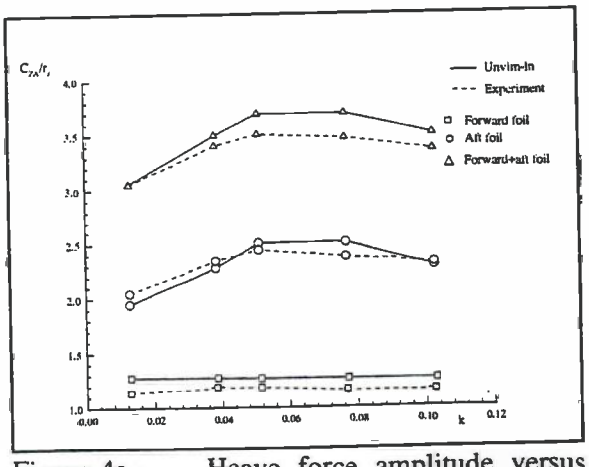


Figure 4a Heave force amplitude versus reduced frequency

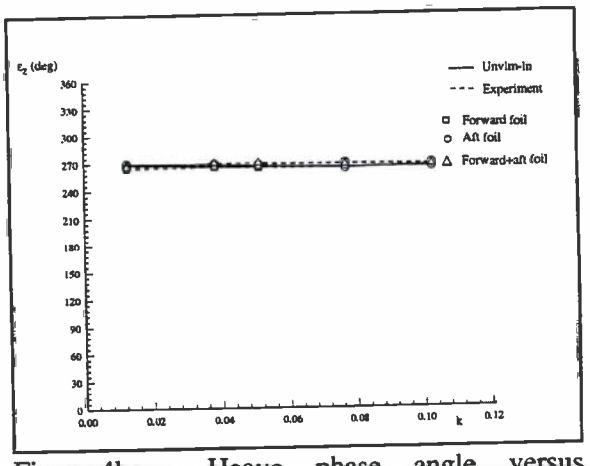


Figure 4b Heave phase angle versus reduced frequency

Figures 4a-d show the vertical force and pitch moment amplitude and their phase angles for an oscillatory heave motion. Unvlm-ln denotes results obtained with the linear unsteady vortex lattice method. These quantities are given for the forward foil, the aft foil and the forward plus aft foils. It

is seen that the vertical force and pitching moment amplitudes are fairly well predicted. There appears a tendency to overpredict the damping which could be attributed to scale effects. The force and moment coefficients for the forward foil are independent of the reduced frequency. For the aft foil some dependency on the reduced frequency is observed, which is most likely due to foil interaction. This is shown in Figure 5 where calculated aft foil results are given with and without foil interaction. Without foil interaction the heave force amplitude is only weakly dependent on the frequency, with interaction the experimentally observed dependency is also shown by the calculation results.

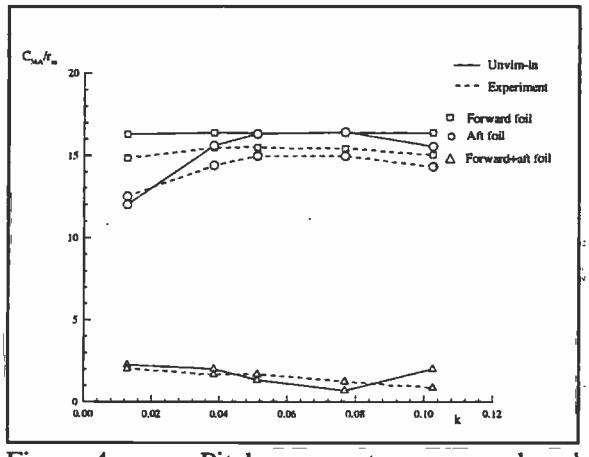


Figure 4c Pitch moment versus reduced frequency

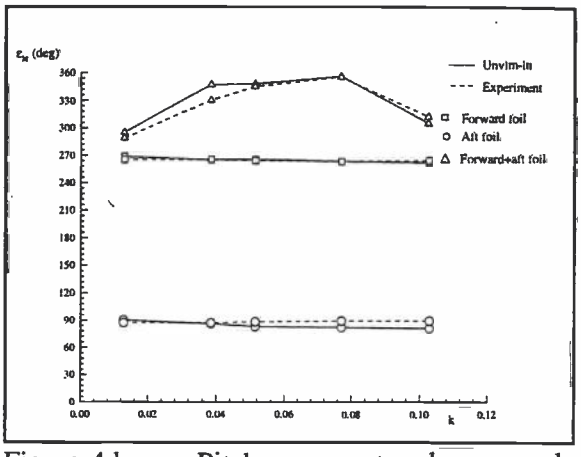


Figure 4d Pitch moment phase angle versus reduced frequency

The phase angles are well predicted. For the pitching moment, the contributions due to the forward and aft foil vertical forces have almost equal amplitudes but also an opposite phase (180 deg difference). Therefore, the forward plus aft foil pitching moment has a small magnitude and a phase angle which can be offset by 90 degrees, relative to the phase angles for the individual pitching moments.

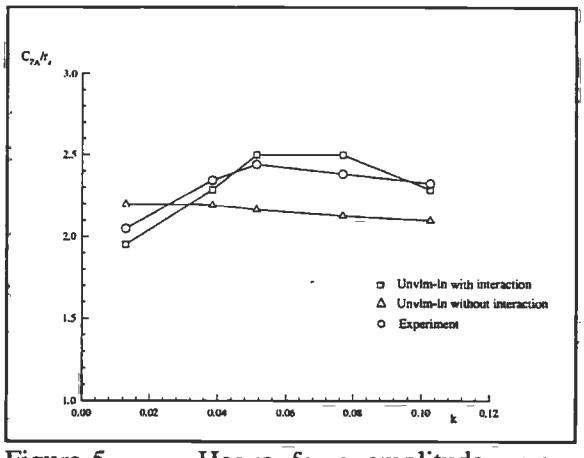


Figure 5 Heave force amplitude versus reduced frequency for aft foil with and without interaction

**Validation case 1: Seakeeping of a surface piercing hydrofoil**

Sferrazza et al. (1992) provide full scale measurement data of the performance of a Rodriquez RHS-160F surface piercing hydrofoil craft in waves. This craft features two surface piercing hydrofoil systems of the airplane type, see Figure 6. Both foil systems are equipped with trailing edge flaps for controlling the roll and pitch motions.

The measurements were performed at deep water (Gulf of Naples) in head, beam and following seas. A wave buoy equipped with accelerometers was used to obtain time registrations of the wave elevations in the measurement area. Accelerometers were installed at the craft to measure the vertical accelerations at the centre of gravity, at the bow and at the stern. Furthermore, the roll and pitch angles

were measured by means of rate gyro's. The speed of the craft during the measurements was 35 knots. The measurements had an average duration of 4 minutes, corresponding to approximately 300, 150 and 70 wave encounters for head, following and beam sea directions respectively. The measurements were performed at a sample rate of 20 Hz. Experience at MARIN shows that for obtaining statistically reliable results, at least 180 wave encounters are needed. Therefore, the results for especially beam wave conditions may not be fully reliable.

The purpose of the trials was to investigate the comfort in various wave conditions in comparison to a catamaran. For this purpose the vertical accelerations and their frequency are the most interesting quantities.

By means of statistical analysis the significant wave height and the zero up-crossing period were determined for each wave height registration based on the wave buoy measurements by Sferrazza et al. (1992). As the time series of the wave elevations buoys were not available, the spectral shapes were assumed to be of the mean Jonswap type. This spectrum type is often used for the type of waves encountered during the trials: wind waves in a sheltered area. The spectra were used in Hydsim to generate time series of the wave elevation and wave orbital velocity components. The spectra were represented by 40 frequency intervals. The Hydsim simulations had a duration sufficient for 200 wave encounters. The actual ride control system used during the trials was incorporated in Hydsim.

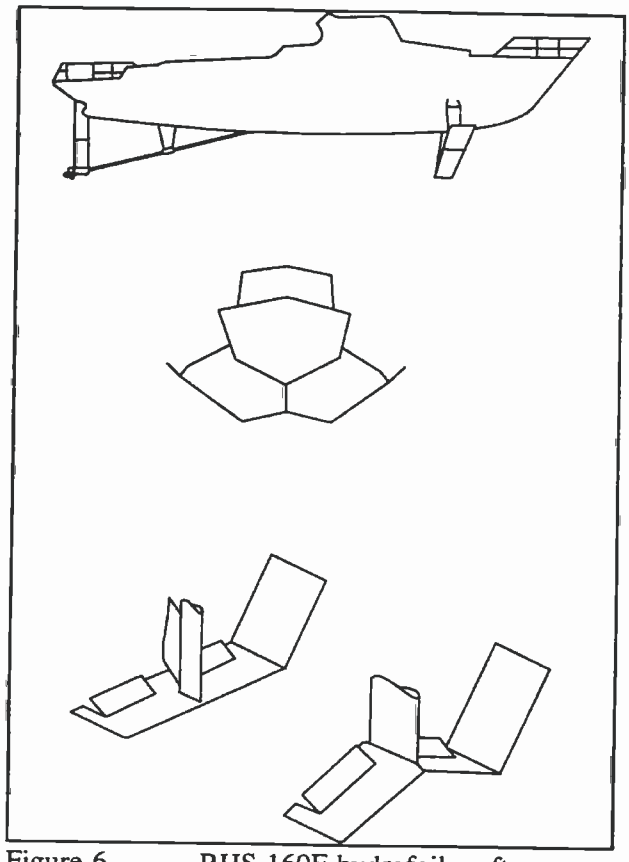

Figure 6 RHS-160F hydrofoil craft

Before focusing on the comparison between the trials and simulation data, some remarks on the trials data are made. The trails data are shown in Tables 1a and 1b on the left side of each column. The wave periods and amplitudes are quite small and are typical for wind generated waves in sheltered regions. In such conditions motion amplitudes of hydrofoil craft are small, which is reflected by the trials data. The motion amplitudes may be contaminated with relatively large noise components. However, the standard deviations of the accelerations are considered to be significant and affect the comfort. It is furthermore noted that for the two beam wave conditions there appears a considerable variation in the trials data. Such differences may be attributed to the randomness of the sea and variations in the wave direction, wind velocity and wind direction, in combination with the relatively low number of wave encounters and the coursekeeping by a helmsman. For these reasons, the emphasis on the validation will be on the vertical accelerations.

Tables 1a and 1b show a comparison between the trials data and the Hydsim simulation results based on the non-linear simulation method Unvlm-nl. In the non-linear method wetted area variations are taken into account due to the craft motions only.

Table 1a Comparison non-linear calculation results for RHS-160F craft "Aldebaran"

| $\psi_w$ | $H_{1/3}$ (m) | $\sigma_\theta$ (deg) | $\sigma_\phi$ (deg) | $\sigma_{accG}$ ($g$) | $\sigma_{accB}$ ($g$) | $\sigma_{accS}$ ($g$) |
|---|---|---|---|---|---|---|
| 180 | .84 .83 | .39 .36 | .58 .00 | .065 .051 | .110 .117 | .110 .092 |
| 0 | .89 .87 | .38 .55 | .98 .00 | .093 .077 | .110 .120 | .120 .125 |
| 270 | .70 .72 | .30 .23 | .50 .45 | .040 .039 | .052 .053 | .056 .048 |
| 90 | .70 .71 | .24 .23 | .24 .45 | .046 .039 | .057 .053 | .066 .048 |

Table 1b Comparison non-linear calculation results for RHS-160F craft "Aldebaran"

| $\psi_w$ | $T_2$ (sec) | $T_\theta$ (sec) | $T_\phi$ (sec) | $T_{accG}$ (sec) | $T_{accB}$ (sec) | $T_{accS}$ (sec) |
|---|---|---|---|---|---|---|
| 180 | 3.50 3.57 | 3.82 2.70 | 3.80 0.00 | 0.82 0.97 | 0.83 0.72 | 0.74 0.56 |
| 0 | 3.60 3.78 | 3.01 2.87 | 3.30 0.00 | 1.54 1.25 | 1.30 1.05 | 1.23 1.12 |
| 270 | 3.70 3.68 | 4.60 3.75 | 3.40 3.25 | 1.33 1.53 | 1.33 0.92 | 0.85 0.77 |
| 90 | 3.90 3.81 | 5.10 3.75 | 3.06 3.25 | 1.45 1.53 | 1.45 0.92 | 1.09 0.77 |

In the columns, the numbers on the left are the trials data while the numbers on the right are the calculated values. Furthermore, $\psi_w$ is the wave direction ($\psi_w$=180 denotes a head sea condition), $H_{1/3}$ is the significant wave height, $\sigma$ is the standard deviation and the subscripts $\theta$, $\phi$, accG, accB and accS denote the pitch and roll motions and vertical acceleration at the centre of gravity, bow and stern respectively. $T_2$ denotes the zero-upcrossing period which is the average value for the period inbetween the upward zero crossings of the signals.
It is seen that with the non-linear method a good agreement with the trials data is obtained. The dependence of the acceleration levels on the wave direction is well predicted. The magnitude of the differences between the zero up-crossing periods for the angular motions and the accelerations are generally well predicted although differences remain for instance the pitch period in beam wave conditions.

Tables 2a and 2b show a comparison between calculation results based on the linear method. Force variations due to changes in the wetted surface of the foil system, caused by the craft motions and wave elevation, are not taken into account in the linear method. It is seen that the accelerations are significantly underpredicted by the linear method. The zero- upcrossing periods for the accelerations in beam seas are not well predicted either.

Table 2a Comparison linear calculation results for the RHS-160F craft "Aldebaran"

| $\psi_w$ | $H_{1/3}$ (m) | $\sigma_\theta$ (deg) | $\sigma_\phi$ (deg) | $\sigma_{accG}$ ($g$) | $\sigma_{accB}$ ($g$) | $\sigma_{accS}$ ($g$) |
|---|---|---|---|---|---|---|
| 180 | .84 .83 | .39 .20 | .58 .00 | .065 .032 | .110 .081 | .110 .088 |
| 0 | .89 .87 | .38 .61 | .98 .00 | .093 .023 | .110 .042 | .120 .044 |
| 270 | .70 .72 | .30 .03 | .50 .48 | .040 .027 | .052 .028 | .056 .028 |
| 90 | .70 .71 | .24 .03 | .24 .48 | .046 .027 | .057 .028 | .066 .028 |

Table 2b Comparison linear calculation results for the RHS-160F craft "Aldebaran"

| $\psi_w$ | $T_2$ (sec) | $T_\theta$ (sec) | $T_\phi$ (sec) | $T_{accG}$ (sec) | $T_{accB}$ (sec) | $T_{accS}$ (sec) |
|---|---|---|---|---|---|---|
| 180 | 3.50 3.57 | 3.82 1.71 | 3.80 0.00 | 0.82 0.96 | 0.83 0.98 | 0.74 1.05 |
| 0 | 3.60 3.78 | 3.01 5.40 | 3.30 0.00 | 1.54 1.70 | 1.30 1.50 | 1.23 1.39 |
| 270 | 3.70 3.68 | 4.60 4.47 | 3.40 5.09 | 1.33 4.23 | 1.33 4.27 | 0.85 5.13 |
| 90 | 3.90 3.81 | 5.10 4.47 | 3.06 5.09 | 1.45 4.23 | 1.45 4.27 | 1.09 5.13 |

For the foil systems used on the RHS-160F type of craft, the dihedral angle of the tip foil parts is about 30 deg which means that a certain submergence variation in the vertical plane results in a wetted length variation which is twice as large. Furthermore, the chord of the tip foil parts is relatively large for the forward foil. These facts suggest that the neglect of wetted area variations in the linearized method might be responsible for the poor predictions.

It can be concluded that the non-linear method can be used successfully for investigating the comfort of surface piercing hydrofoil craft under normal operating conditions. The main reason for the linear method to give inadequate predictions is the neglect of wetted surface variations. These variations are due to the craft motions and the wave elevations. For the present case, and hydrofoil craft in general, wave amplitudes are an order of magnitude larger than the craft motion amplitudes. Including the correction on the foil lift force accounting for the wetted surface variation due to the wave elevation in the linear method can therefore be expected to significantly improve its predictions for surface piercing hydrofoil craft.

**Validation case 2: Seakeeping and manoeuvring of a fully submerged hydrofoil craft**

Saito et al. (1991) provide seakeeping data for the Jetfoil-115 type hydrofoil craft. This hydrofoil craft has a fully submerged foil system with a canard foil area distribution, see Figure 7. The craft is equipped with a ride control system actuating trailing edge flaps at the forward and aft foil systems. Directional stability is obtained from the forward strut which acts as a rudder. Several sensors are used to obtain control system input. The relations between input and output signals have been obtained from Saito et al. (1991) on basis of calculated values for the hydrodynamic derivatives of the craft. These relations include corrections for the actuation of flaps.

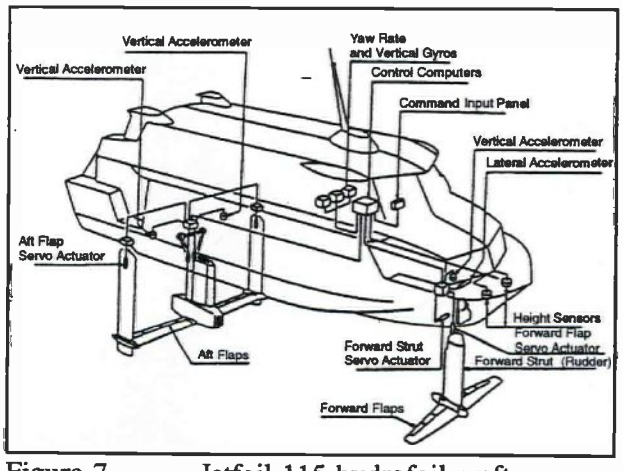

Figure 7 Jetfoil-115 hydrofoil craft

The relative hull clearance at the bow, the vertical acceleration at the bow and the forward foil flap angle were recorded during one month of commercial operation in the Japan Sea. The measured data show a significant scatter for a constant wave height, which is likely due to the variation in the waveperiods encountered during the trials period. This variation in wave conditions is often expressed in wave scatter diagrams which shows the probability of occurrence of a certain combination of wave height and wave period for a certain location on sea in a certain season. For the Hydsim simulations

such a scatter diagram for the Japan Sea was used to determine the two mean wave period ranges with the highest probability, for a series of significant wave height values. For the mean value in each wave period range simulations with Hydsim were carried out, both on basis of the linear and non-linear methods. The conditions thus described cover approximately 50% of the wave height-wave period combinations present in the scatter diagram, for wave heights up to 2.0 m.

The simulation results are shown in Figures 8a-c. Non-linear results (Unvlm-nl) are somewhat closer to the mean value of the trials data than linear simulation results. The differences between the linear and non-linear results are however much smaller than for the earlier described surface piercing hydrofoil craft. Above a wave height of 1.5 m the simulation results start deviating from the trials mean line. This may be due to cavitation, but also the manual depth control is of influence here.

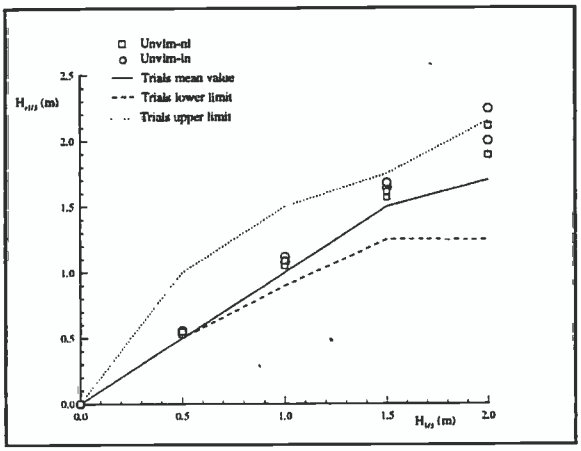


Figure 8a Significant relative hull clearance at bow

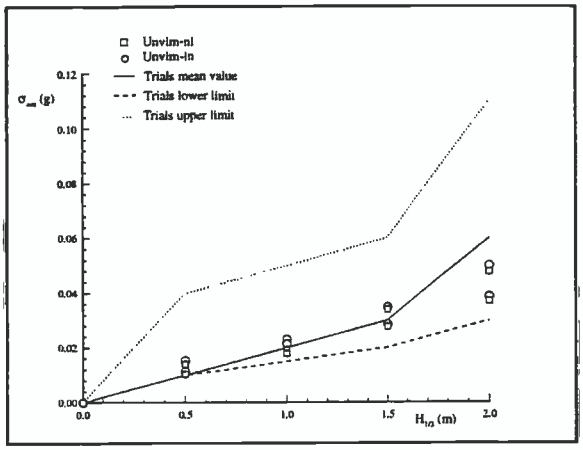


Figure 8b Standard deviation of vertical acceleration at bow

Figure 8d finally shows a comparison for the manoeuvring behaviour of the Jetfoil. The trials data are obtained from Saito et al. (1990). The Figure shows a coordinated turning manoeuvre whereby the helmsman suddenly sets a certain "helm command" proportional to the required yaw rate. At this command, the entire forward foil is rotated (strut angle) and the craft assumes a certain roll angle and yaw rate. It is seen that there exists a fair agreement between the trials data and the non-linear simulation data. The roll angle during the turn is reasonably well predicted, but in the simulation the roll response of the craft is too fast. The same holds for the yaw rate and the lateral acceleration at the bow. This discrepancy may perhaps be caused by wave disturbances during the trials. These are present at least before the start of the manoeuvre where the strut angle is equal to zero.

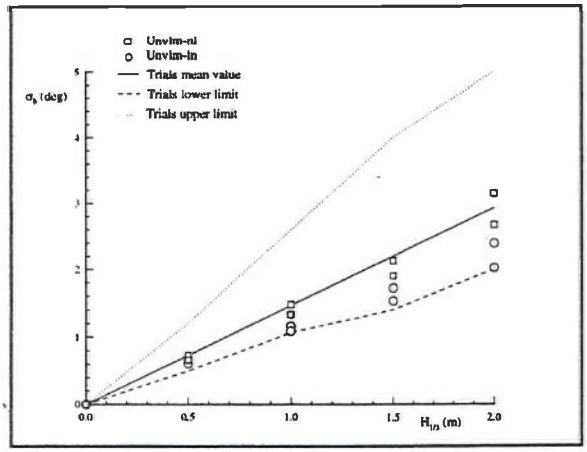


Figure 8c Standard deviation of forward flap angle

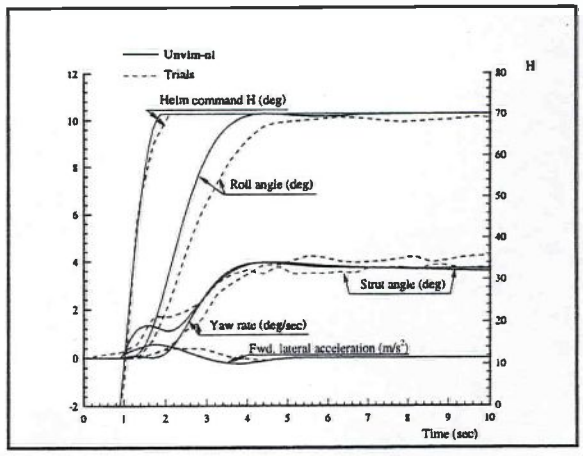


Figure 8d Turning manoeuvre

**Acknowledgement**

Rodriquez Engineering Srl. and Kawasaki Heavy Industries Ltd. are thanked for their permission to use the full scale data of their hydrofoil craft.

**References**

Newman J.N. (1985), 'The Evaluation of Free-Surface Green Functions', Fourth International Conference on Numerical Ship Hydrodynamics, Washington, pp. 4-19.

Newman J.N. (1992), 'The Approximation of Free-Surface Green Functions', In: P.A. Martin and G.R. Wickham, editors, Wave Asymptotics, Cambridge University Press, pp. 107-135.

Lin W.M. and Yue D. (1990), 'Numerical Solutions for Large-Amplitude Ship Motions in the Time Domain', Proceedings of the 18th Symposium on Naval Hydrodynamics, Ann Arbor, pp. 41-65.

Saito Y. et al. (1990), 'Fully Submerged Hydrofoil Craft', 7th Marine Dynamics Symposium, Society of Naval Architects of Japan, Japan.

Saito Y., Oka M., Ikebuchi and Asao M., (1991), 'Rough Water Capabilities of Fully Submerged Hydrofoil Craft Jetfoil', First International Conference on fast Sea Transportation, Trondheim, pp. 997-1012.

Sferrazza M., Di Blasi D. and Buccini C. (1992), 'Dynamic behaviour: A Comparison Between Hydrofoil and Catamaran', in: Hydrodynamics: Computations, Model tests and Reality, H.J.J. van den Boom (Editor), Elsevier Science Publishers B.V., the Netherlands.

Van Walree F. (1999), 'Computational methods for hydrofoil craft in steady and unsteady flow', Thesis at Technical University of Delft, the Netherlands.